Synopsis of the thesis

Numerical Investigation on Flow and Heat Transfer from Porous Bluff Bodies using Lattice Boltzmann Method

By

T. R. Vijaybabu

(Roll No. 1501103003)

Under the Supervision of

Dr. Shanmugam Dhinakaran

DISCIPLINE OF MECHANICAL ENGINEERING

INDIAN INSTITUTE OF TECHNOLOGY, INDORE, INDIA

February 2018

1. Introduction

The remarkable development in miniaturisation and performances of thermal devices and increasing use of Multi-Chip-Module (MCM) in electronics demand reliable thermal control methods. The temperature regulation has become indispensable in order to guarantee the optimum performance of a system for a stipulated period of time. Several active and passive approaches have been suggested and implemented for enhancing the heat transfer characteristics [1]. Amongst various passive techniques for augmenting heat dissipation, employing higher thermal conductivity fluids (nanofluids), increasing the surface area of the component and utilizing porous medium are popular. Numerous studies related to porous medium [2–4] suggest that the heat transfer performance of a system can be extensively improved by using porous material with higher thermal conductivity. The utilization of intrinsic feature of the porous medium is being widely used in many environmental and engineering applications such as packed bed heat exchangers, drying technology, catalytic reactors, thermal insulation, petroleum industries, tissue engineering and electronic cooling [5, 6]. On the other hand, a complex system with numerous elements arranged orderly can be considered as a single porous body [7]. This empowers the researchers and/or engineers to discover experimentally unapproachable problems with significant computational economy. Few relevant examples are arrangement of fuel and control rods in nuclear reactor core, pin-fin arrangement, LED backlit module and heat exchanger. Such arrangements can be tuned to receive required flow and thermal characteristics. This exemplifies the reason for trending of the research on porous media and associated modeling theory.

2. Motivation

The modeling of different thermal systems using porous media towards optimal heat transfer requires the knowledge on various influencing parameters such as momentum, buoyancy, magnetic field, alignment and size of the porous body. Also, the combined effects of aforementioned parameters are expected to produce a notable impact on the designing of permeable bluff bodies. Thus, understanding the impression of these factors is one of the main driving forces for research in flow and heat transfer from porous bluff bodies. Moreover, the recent literature survey indicates the paucity of education in this field. Key observations from the available literature are (*i*) the unsteady flow and heat transfer characteristics of a porous bluff body with different fore-body and aft-body are not studied, (*ii*) the influence of aiding buoyancy condition on hydrothermal behaviour of bluff body is not probed, (*iii*) the buoyancy and permeability interaction along with fore-body effects on hydrodynamic and thermal dissipation of porous bluff body has yet not been estimated, (*iv*) natural convection characteristics of porous bluff body have been not reported and (*v*) the influence of magnetic field and nanofluid on natural convection characteristics of porous bluff body are also not available. Apart from these observations, the lattice Boltzmann method (LBM), which has a significant advantage over convectional numerical methods (especially while dealing with complex flows such as porous media) [8], has not been employed to study the flow and heat transfer traits of porous bluff bodies.

3. Objectives of the present study

The objectives of the present study are as follows:

1. To investigate unsteady flow and heat transfer from a diamond-shaped porous bluff body.

2. To study the influence of aiding buoyancy on flow and thermal traits of square-shaped porous bluff body.
3. To probe the effect of aiding buoyancy and orientation on hydrodynamic and thermal characteristics of a permeable triangular cylinder.
4. To analyse natural convection heat transfer behaviour of square-shaped porous body for different aspect ratios and orientations.
5. To examine the magnetohydrodynamic natural convection heat transfer phenomenon of a permeable triangular cylinder for two different orientations with nanofluid.

The above analyses are carried out by employing LBM in which the transport equations are solved at mesoscopic scale level.

4. Results and discussions

Results obtained after carrying out numerical endeavours on the above mentioned objectives are detailed in the forth-coming sub-sections.

4.1. *Unsteady flow and heat transfer from a diamond-shaped porous cylinder*

In this analysis, the unsteady flow and heat transfer around a diamond-shaped porous cylinder placed in an infinite stream of fluid have been numerically analysed using LBM. The variations in hydrothermal behaviour of the porous cylinder have been studied for different values of Darcy number ($10^{-6} \leq Da \leq 10^{-2}$) and Reynolds number ($50 \leq Re \leq 150$). The computational domain used in this study along with LB boundary conditions can be visualised in Fig. 1.

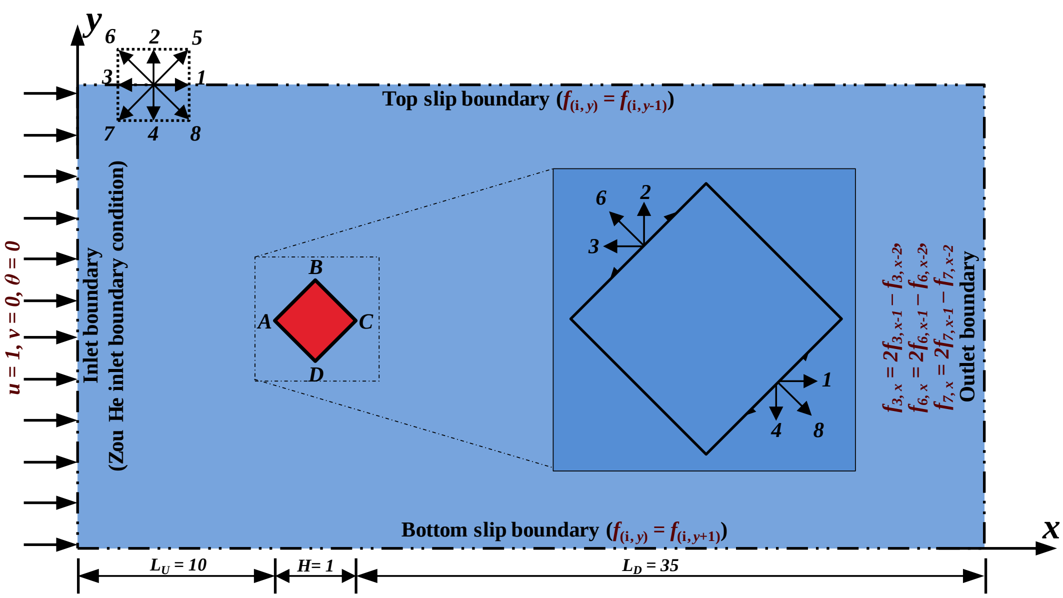

Figure 1: Computational domain for the unsteady flow and heat transfer from a porous diamond-shaped cylinder.

A substantial reduction in vortex shedding strength is witnessed for the same momentum of the fluid with higher permeability. The evaluated lift coefficients at each time instants can be visualised in Figs. 2(a) and (b) at start of vortex flow and dynamic steady state, respectively, for different values of Da at $Re = 100$.

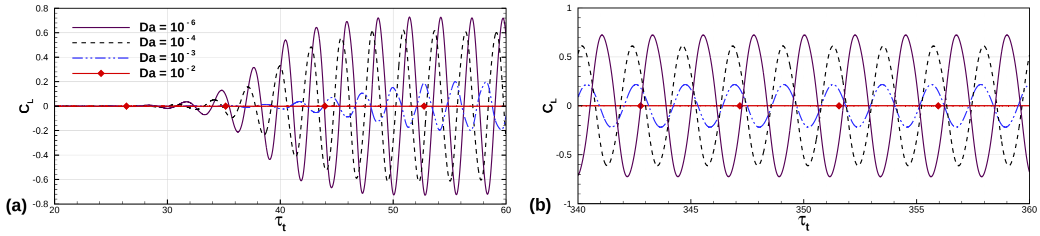

Figure 2: Time evolution of lift coefficient (C_L) at (a) start of vortex flow and (b) dynamic steady state for different values of *Da* and at *Re* = 100 for flow around and through a diamond-shaped porous cylinder. Legend in (a) is also applicable to (b).

It can be seen that the lift oscillations occur for $Da = 10^{-3}$ later than 10^{-4} and 10^{-6} with less amplitude. This implies that the vortex shedding appearance can be delayed by increasing the permeability value. A finite amount of fluid which enters into the permeable cylinder reduces the resultant pressure and shear forces acting in the direction normal to the flow. Hence, the amplitude of oscillation is observed to be greater under lower permeable condition with relatively lower frequency of oscillation. Moreover, the permeable square-shaped body produces flow instabilities which is found to be absent in porous diamond-shaped cylinder. Reduction in drag, and heat transfer augmentation in overall heat transfer are seen while enhancing the permeability of the cylinder. The variation of time-averaged mean Nusselt number at different values of *Da* and *Re* have been presented in Fig. 3(a). At $Da = 10^{-4}$, due to large deviation in fluid path and less fluid velocity in porous region, the heat transfer rate is less significant than other higher values of non-dimensional permeability values. The low values of temperature gradient on frontal surfaces of the cylinder at rich permeable values (i.e. $Da = 10^{-2}$), dominates over low heat dissipation rate of rear surfaces. As a result of this, the heat transfer enrichment is drastic for this permeability range. Correlations for time-averaged mean Nusselt number, valid for the range of parameters considered are also provided, and this indicates the strong influence of momentum on heat transfer increment than permeability. Furthermore, a comparative study on thermal dissipation from the permeable square and diamond shaped cylinders is carried out at *Re* = 50, 100 & 150 at different values of *Da* and it can be seen in Fig. 3(b).

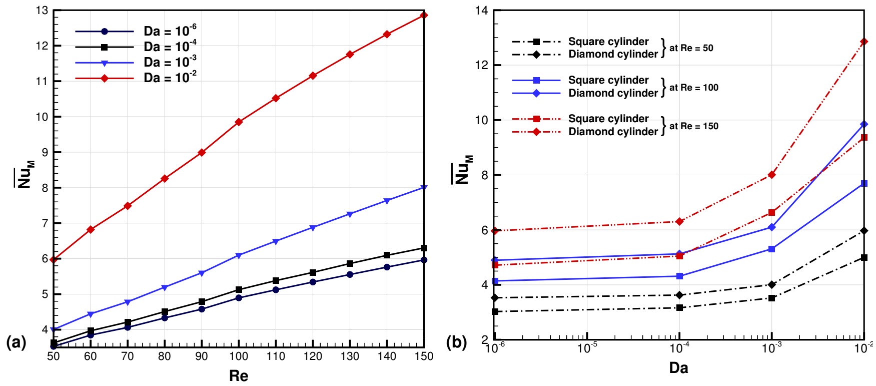

Figure 3: (a) Effect of *Da* on time-averaged mean Nusselt number ($\overline{Nu_M}$) at different values of *Re* (50≤ *Re* ≤150) for flow around and through a permeable diamond-shaped cylinder; (b) Time-averaged mean Nusselt number ($\overline{Nu_M}$) comparison between permeable square and diamond-shaped cylinder at *Re* = 50, 100 and 150 for different values of *Da*.

It is to be noted that in case of permeable cylinder, while increasing the *Da*, the thinning and thickening of thermal boundary layer are noticed at windward and leeward surfaces, respectively. Albeit, the square-shaped cylinder has only one leeward surface, its thermal performances are seen to be lower than that of diamond-shaped cylinder (refer Fig. 3(b)). Further, due to the dominance of thick thermal boundary layer formation at rear surfaces of diamond-shaped cylinder, the percentage increment in mean Nusselt number of the diamond-shaped cylinder with reference to square decreases monotonously with the increase of non-dimensional permeability. For example, at $Re = 100$, the percentage enhancement of diamond-shaped cylinder at $Da = 10^{-6}$, 10^{-4}, 10^{-3} and 10^{-2} is 15.87%, 15.37%, 12.95% and 21.84%, respectively, with reference to permeable square cylinder. At $Da = 10^{-2}$, the influence of frontal surfaces is more than rear surfaces and thus, at this condition the percentage enhancement of diamond-shaped cylinder is high. Broadly, from this study we have seen that the increment in permeability reduces flow instabilities as well as enriches thermal performances in comparison to square shape. Thus, while modeling porous bodies or a group of bodies for pragmatic applications the alignment and permeability level have to be considered.

4.2. Mixed convection heat transfer from permeable square cylinder

From literature, it is evident that the mixed convection characteristics can greatly alter the flow and thermal behaviour in the vicinity of heated cylinder. In particular, the aiding buoyancy condition intensifies the thermal performances and also it suppresses the flow instabilities [9]. In this regard, we have conducted numerical experiments to study the hydrodynamic and thermal behaviour of permeable square cylinder under aiding buoyancy condition. *Re* and *Da* values considered in this study vary from 2 to 40 and 10^{-6} to 10^{-2}, respectively. The flow and heat transfer traits at Prandtl number (*Pr*) value of 0.71 is compared for three different values of Richardson number (*Ri*) i.e. 0, 0.5 and 1. The computational setup employed in this analysis is shown in Fig. 4.

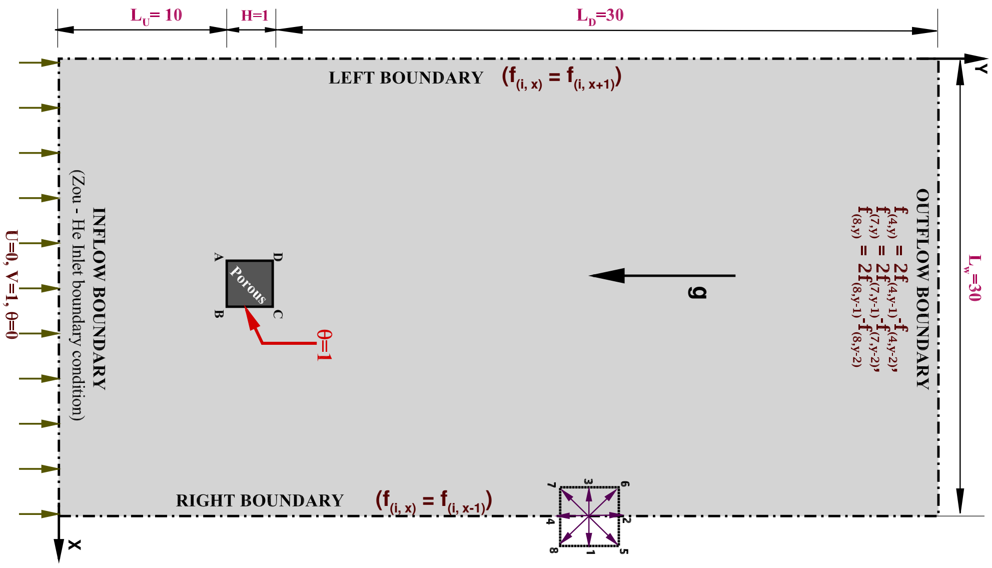

Figure 4: Computational domain used in the analysis of mixed convection flow and heat transfer from a porous square cylinder.

In general, the flow and heat transfer characteristics are found to be a function of non-dimensional permeability or *Da*, buoyancy condition and *Re*. It is observed that a monotonous reduction in wake length and drag coefficient values occurs at higher permeability levels. On the other hand, aiding buoyancy depicts a pronounced reduction in wake length and an increment in drag coefficient values. Also, the excess viscous force of the porous zone at lower *Da* (i.e. $Da = 10^{-6}$) offers resistance to the flow movement through it irrespective to the value of *Re* and *Ri* embraced in this study. At this level, the permeable cylinder mimics its solid body counterpart in terms of both flow and thermal characteristics. Further increment in permeability causes dominance of inertial force over the viscous force of porous medium, and hence, fluid flows through it with different deviation levels. The deviation of flow in the porous zone is found to be less while increasing the permeability for same fluid momentum. Besides, the permeability increment reduces the pressure over the cylinder and more amount of fluid is noticed to be attached over it. Conversely, the buoyancy increment reduces the flow path deviation in the cylinder and the same can be seen in Fig. 5.

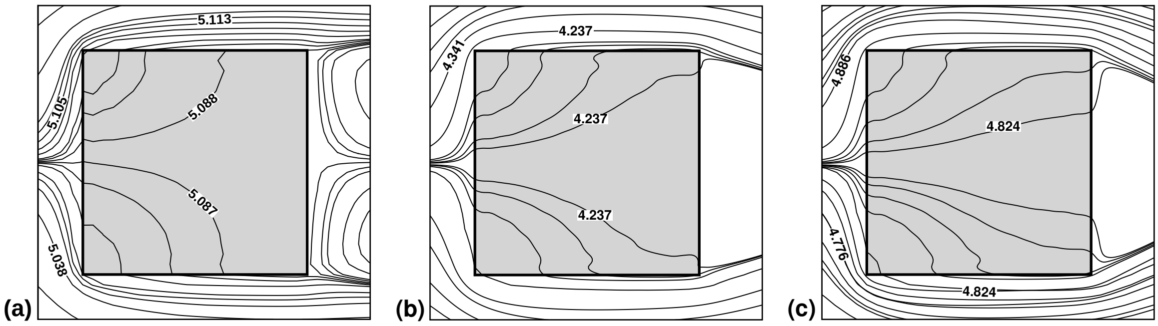

Figure 5: A closer view of streamline pattern through the permeable cylinder at $Re = 40$ and $Da = 10^{-4}$ for (a) $Ri = 0$, (b) $Ri = 0.5$ and (c) $Ri = 1$.

A significant augmentation in heat dissipation is reported for increasing values of *Ri* and/or *Da*. The permeability increment stretches the isotherms and also reduces the temperature gradient at side surfaces. Whereas, *Ri* significantly enhances the temperature gradient which is evident from the narrow isotherms. Moreover, the increment in buoyancy level enhances the impact of permeability on heat transfer enhancement. For instance, the percentage increase in mean Nusselt number at $Re = 40$, $Da = 10^{-4}$ at $Ri = 0$, 0.5 and 1 is 2.04%, 2.2% and 3.03%, respectively, in comparison to $Da = 10^{-6}$ case. Furthermore, the heat transfer intensification is prominent while *Ri* shifts from 0 to 0.5 and it is less sensitive while it varies from 0.5 to 1.

4.3. Mixed convection heat transfer from permeable triangular cylinder

In this investigation, we have concentrated on the fore-body and aft-body influence on hydrothermal behaviour of porous bluff body under aiding buoyancy condition. The combination of flat and slant edges of the triangular cylinder, has shown impressive heat transfer characteristics than square shape [10]. On this subject, we have chosen the shape of the permeable body as triangular which is aligned at two different orientations (i.e. apex facing flow and side facing flow). Objective of this study is to investigate the effects of *Da* and fore-body shape on flow and heat transfer characteristics, under forced convection (i.e. $Ri = 0$) and aiding buoyancy conditions (i.e. $Ri = 0.5$ & 1) for $Pr = 0.71$. The ranges of *Re* and *Da* considered in this study are $1 \leq Re \leq 40$ and $10^{-6} \leq Da \leq 10^{-2}$, respectively.

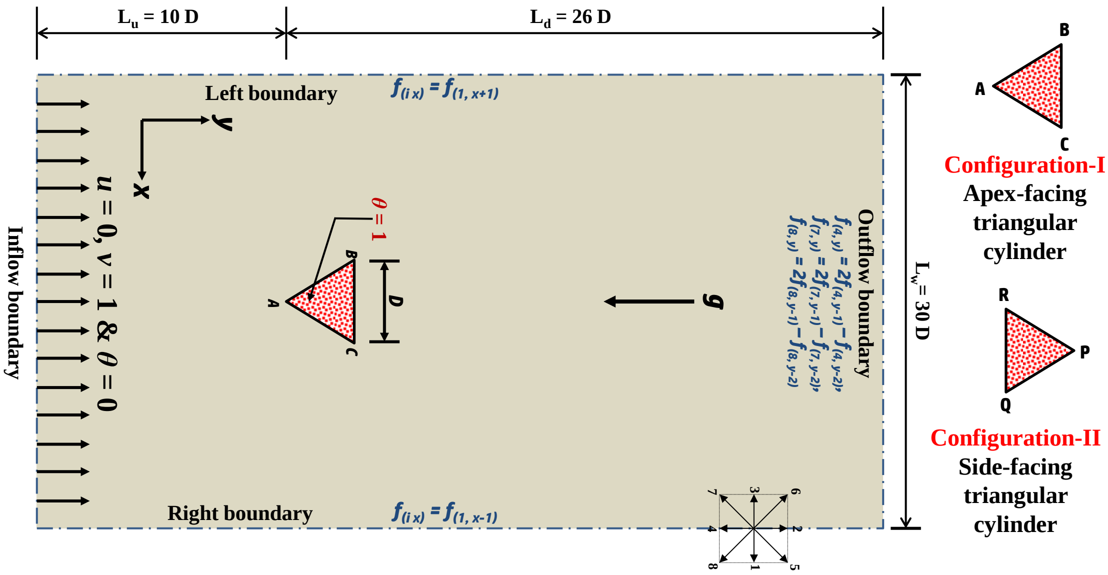

Figure 6: Computational domain used for mixed convection flow and heat transfer from a permeable triangular cylinder. Apex and side facing triangular cylinder configurations are also shown in figure.

The computational domain used in this investigation is presented in Fig. 6. The flow deviation produced by apex facing triangular cylinder is lesser than that of side facing flow. This is due to the less viscous force acting on the fore-body of the former configuration. Also, at higher Ri (i.e. $Ri = 1$) the flow is completely attached over the side facing configurations for all values of Re and Da. However, apex facing triangular cylinder has produced flow separation and it is due to the enhancement in fluid momentum at slant surfaces and sharp corners. The excess viscous force offered by buoyancy is the cause for substantial increment and decrement of drag coefficient and recirculation values, respectively. On the contrary, a more permeable triangular cylinder experiences less drag value with short eddies.

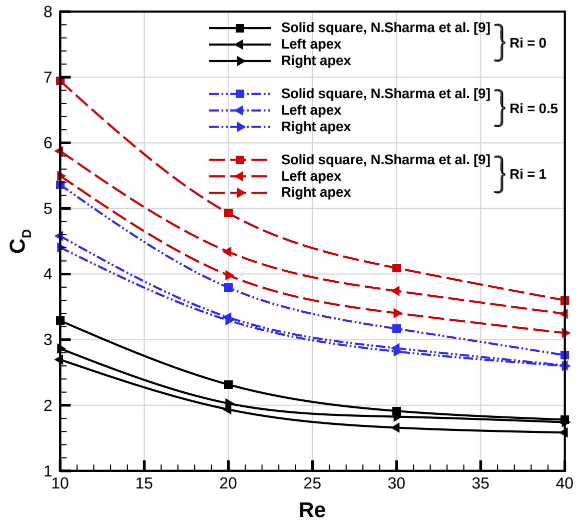

Figure 7: Comparison of drag coefficient (C_D) values of apex facing flow, side facing flow triangular cylinder with square cylinder under different buoyancy levels at $10 \leq Re \leq 40$ and $Da = 10^{-6}$.

We have also compared the drag coefficient values of solid square cylinder with triangular cylinders at different values of Re and Ri which are shown in Fig. 7. For all values of Re

and/or Ri, the drag coefficient of square cylinder is higher than that of triangular configurations. In the absence of buoyancy, the drag coefficient values of side-facing triangular cylinder lie between the square and apex-facing cylinders. Under aiding buoyancy condition, the side facing triangular cylinder experiences less drag than apex facing for all values of Da.

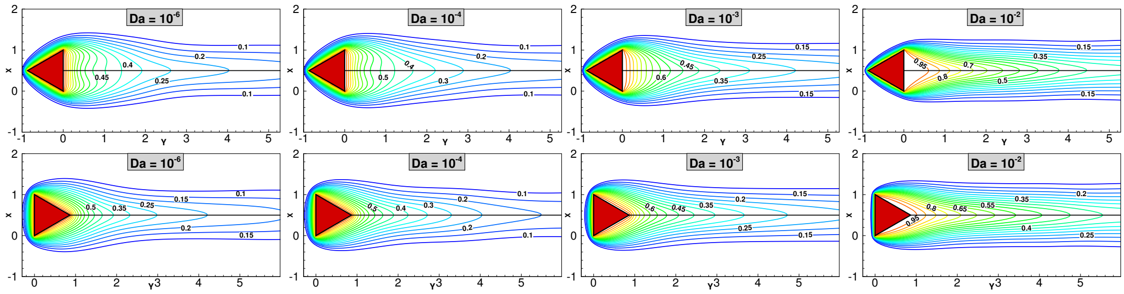

Figure 8: Isotherms at $Re = 40$ and $Ri = 0, 0.5$ and 1 for various Da values for the flow around and through the porous triangular cylinder.

The temperature distribution of apex-facing and side-facing configurations are shown in Fig. 8 for different values of Da at $Re = 40$ and $Ri = 1$. The isotherms are clustered more at slant and side surfaces of the apex-facing and side-facing cylinders, respectively. Also, at downstream the isotherms become narrow which indicates a slight augmentation in temperature gradient at slant surfaces. However, due to the fluid penetration through the cylinder, the isotherms expand in the lateral direction. As a result, the enhancement offered by buoyancy reduces while enriching the permeability. Further, the isotherm value of 0.95 at $Da = 10^{-2}$ indicates the reduction in temperature gradient. Although, this isotherm line of the apex-facing triangular cylinder covers largest area in comparison with side-facing configuration, the overall thermal performance of the former configuration is high. The increment of Re reduces the heat transfer enhancement produced by Ri at wind ward surface for $Da \leq 10^{-4}$. However, this enhancement ratio increases with further increment in Da and it is found to be high at $Da = 10^{-2}$. Also, such heat transfer enhancement of a highly permeable cylinder reduces at very low values of Re. The mean Nusselt number of apex facing triangular cylinder is seen to be higher than that of side-facing configuration irrespective to the variation in Re, Da and Ri.

4.4. *Natural convection heat transfer from porous square body*

This analysis is focused on the natural convection between a hot porous body and the square enclosure in which it is placed. The effects of aspect ratio (A), non-dimensional permeability or Da, Rayleigh number (Ra) and orientation of porous square body on flow and heat transfer characteristics have been extensively analysed. The computational domain and boundary conditions can be seen in Fig. 9. The ranges of Ra and Da considered in this study are $10^3 \leq Ra \leq 10^6$ and $10^{-6} \leq Da \leq 10^{-2}$ for $Pr = 0.71$. The porous body is aligned at two different orientations (i.e. stand-on-side (SOS) and stand-on-edge (SOE)) for the fixed aspect ratio (porous body height/enclosure height) values of 0.5, 0.25 and 0.125.

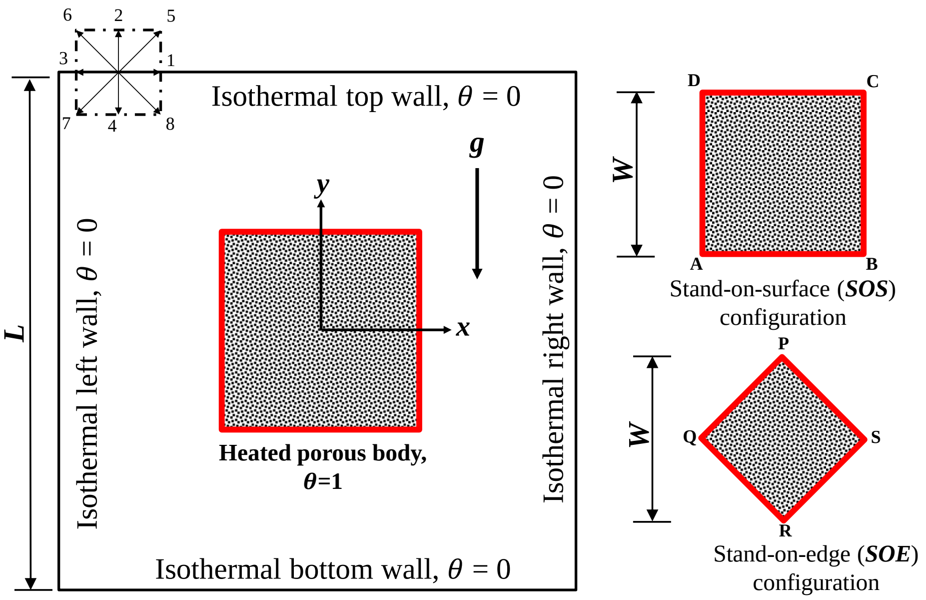

Figure 9: Computational domain used in the analysis of natural convection flow and heat transfer from a porous body. *SOS* and *SOE* configurations are also shown in figure.

It is seen that the flow field dependence on *Ra* and *Da* is less at low values of aspect ratio for both configurations of porous body. At $Da = 10^{-6}$, the porous body completely impedes the fluid flow through it due to the large viscous resistance offered by the body.

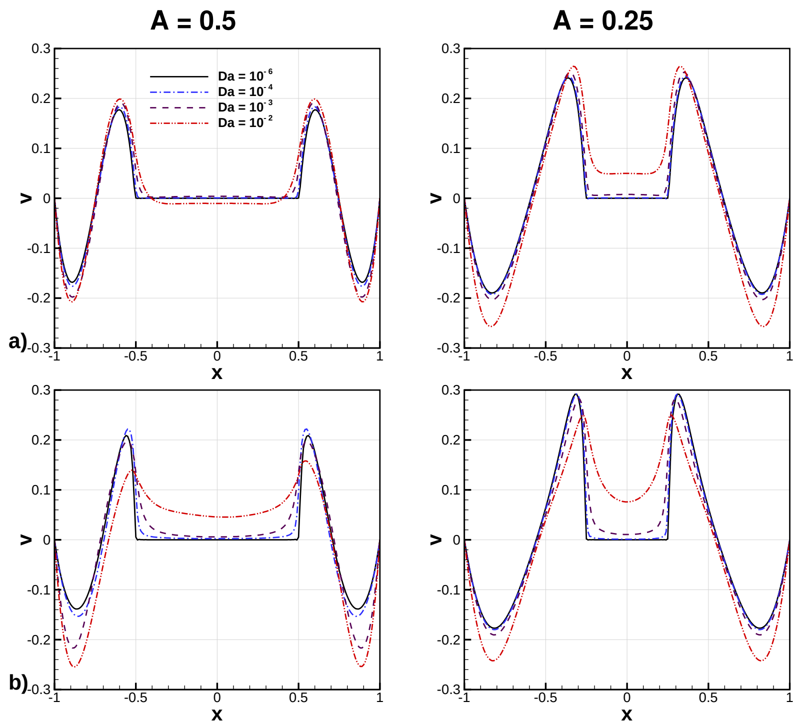

Figure 10: Normal velocity (u-velocity) profile along the x-direction of the square enclosure at $y = 0$ for different values of *Da* and aspect ratio for (a) *SOS* and (b) *SOE* configurations at $Ra = 10^5$. Legend in (a) is applicable to (b).

The variations of vertical velocity (v-velocity) along x-direction of the square enclosure at $y = 0$ due to permeability, aspect ratio are shown in Figs. 10(a) and (b) for *SOS* and *SOE* alignments of the porous body, respectively. The increment in permeability enhances the intensity of velocity in the porous zone for all values of aspect ratio and configuration. In addition, the vertical velocity values with permeability increment is seen to be relatively higher in case of *SOE* configuration than *SOS*. Broadly, it can be inferred that the increment in permeability value enhances the kinetic energy of the fluid in and around the porous zone. Besides, the flow path deviation in the porous zone is seen to be more at $A = 0.5$ of *SOS* configuration, and the same is observed to be minor while reducing the size of the porous body. On the other hand, the increment in *Da* level causes thinning and thickening of thermal boundary layer at bottom and top surfaces of the porous body, respectively. Also, the thermal gradient of side surfaces of *SOS* cylinder is dependent on the aspect ratio.

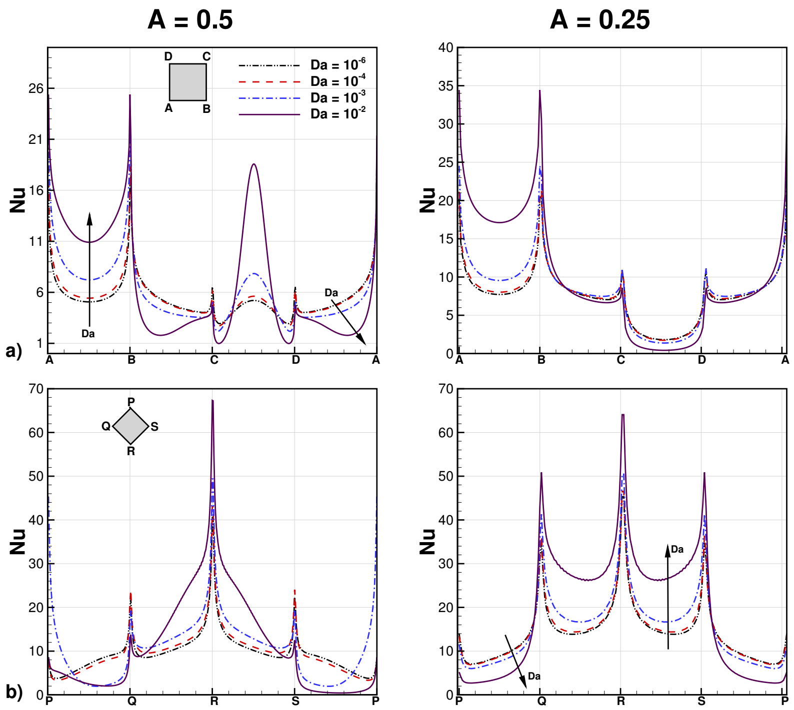

Figure 11: Local Nusselt number distribution along the surface of the porous body at different values of *Da* and aspect ratio for (a) *SOS* and (b) *SOE* alignments at $Ra = 10^5$. Legend in (a) is applicable to (b).

Figs. 11(a) and (b) explore the combined effects of *Da* and aspect ratio on local Nusselt number distribution of porous cylinder at $Ra = 10^5$ for *SOS* and *SOE* configurations, respectively. At higher aspect ratio (i.e. $A = 0.5$), the increment in *Da* improves the Nusselt number values at bottom surface of *SOS* and it depletes the same at side surfaces. At higher permeability the fluid enters through bottom surface and it leaves via side surfaces, and this causes the reduction in heat transfer at side surfaces. Furthermore, the formation of vortices at top portion enhances the thermal gradient of middle portion of top surface at $A = 0.5$. However, such scenarios have not been seen in lower aspect ratio cases. The Nusselt number values of *SOE* configuration are found to be relatively higher than that of *SOS* configuration. The enclosure mean Nusselt number of *SOS* configuration is higher than *SOE* configuration. Thus, it indicates that the enclosure with *SOE* permeable body will contain higher amount of denser or cold fluid.

Furthermore, we have also performed second-law analysis in which the entropy variation with the embraced parameters considered in this study is studied. It is observed that the total entropy value is directly proportional to *Ra* and *Da*, and it is indirect proportional with the aspect ratio.

4.5. Magneto hydrodynamics natural convection heat transfer from porous triangular body with nanofluid

In this study, we have examined the natural convection heat transfer between a hot permeable triangular-shaped cylinder and a cold square enclosure under the influence of magnetic field. Al_2O_3-water nanofluid with 5% volume fraction is considered as a working fluid and the effective thermal conductivity and viscosity values are evaluated through KKL (Koo-Kleinstreuer-Li) correlation. The ranges of *Ra* and *Da* considered in this study are $10^4 \leq Ra \leq 10^6$ and $10^{-6} \leq Da \leq 10^{-2}$, respectively. The flow and thermal characteristics of triangular body for two different alignments (i.e. (*i*) apex facing up and (*ii*) apex facing down) are critically investigated for the aforementioned parameters at different values of Hartmann number (i.e. *Ha* = 0, 25 & 50). The computational setup of this study and different configurations of permeable triangular body can be seen in Fig. 12.

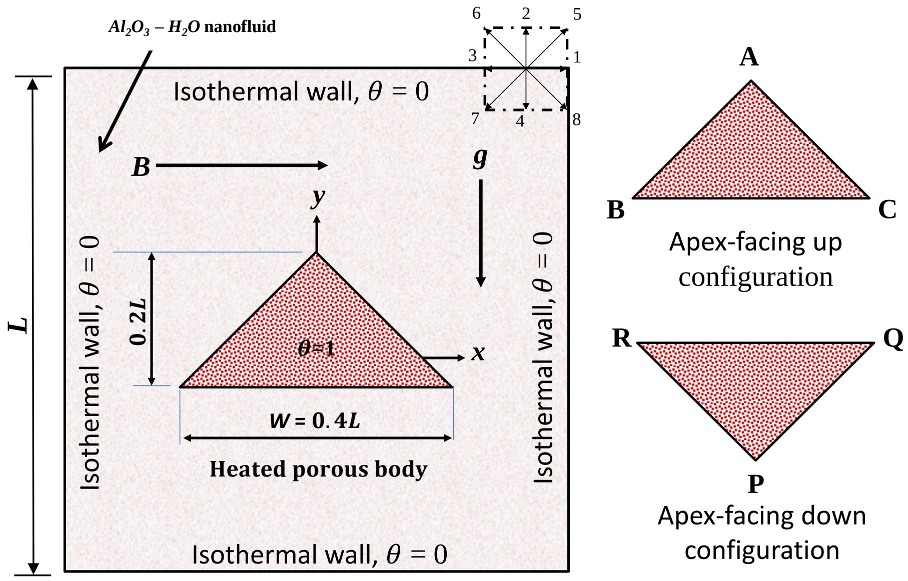

Figure 12: Computational setup used for MHD natural convection flow and heat transfer from a permeable triangular body. Apex facing up and down configurations are also shown in figure.

The flow path through the permeable body is found to be divergent and convergent in style for apex facing up and down configurations, respectively. This is due to the amount of porous zone presents at the windward surface of the triangular body. It is seen that the permeability increment enhances the fluid momentum, whereas, the presence of magnetic field reduces the kinetic energy of the fluid. Presence of magnetic field retards the fluid momentum in the annular space and permeable zone. However, the flow pattern in the porous zone is observed to be similar irrespective to the intensity of magnetic field. Also, the Hartmann number has shown a strong impact on vertical velocity field at annular, whereas, this effect is found to be trivial in porous zone.

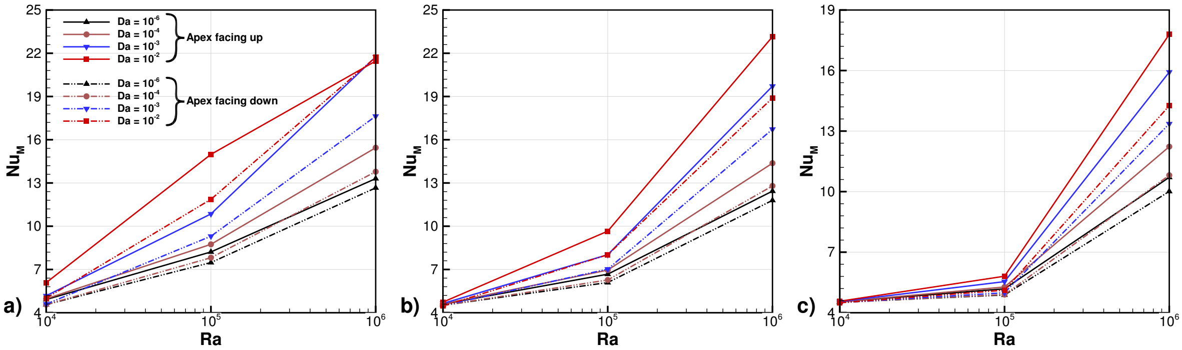

Figure 13: Effect of Ra on mean Nusselt number (Nu_M) of permeable triangular body in two different orientations for different Da values at (a) $Ha = 0$, (b) $Ha = 25$ and (c) $Ha = 50$ with solid volume fraction of 5% for natural convection from a permeable triangular body placed in a square enclosure. Legend in (a) is also applicable in (b) and (c).

The effects of Ra, Da and orientation of the permeable triangular body on mean Nusselt number (Nu_M) are illustrated in Figs. 13(a)-(c). The increment in Ha suppresses the intensity of permeability on heat transfer enhancement. Further, the overall heat transfer of apex facing up triangular configuration are reported to be higher than that of apex facing down configuration for all values of Ra, Da and Ha considered in this study. Further, the effect of heat transfer reduction due to the increment in Hartmann number is prominent at higher values of Da. The mean Nusselt number value increases with the increment in permeability levels and it reduces with Ha increment. Also, the impact of permeability on thermal enhancement is higher in apex facing up permeable triangular body than apex facing down case irrespective to the intensity of magnetic field. On contrary, the heat transfer reduction due to Ha increment is seen to be less in apex facing down configuration at $Ra \leq 10^5$.

5. Conclusions

The major outcomes drawn from this study are summarized as follows:

- Reduction in vortex shedding strength is observed when the permeable square body is aligned to diamond-shape. The thermal enhancement of diamond-shaped permeable body is higher than that of square-shaped cylinder irrespective of the values of Da.

- Aiding buoyancy depletes the viscous resistance offered by permeable body. Consequently, the fluid momentum through the porous zone enhances while augmenting Ri value. Furthermore, the increment in Da increases the temperature gradient at windward surface, and it produces thermal inversion at leeward surface. The presence of buoyancy reduces the thickening of thermal boundary layer at side surfaces of hot permeable body due to the higher amount of attached flow.

- The fore-body of permeable body changes the fluid flow path in the porous zone. The lesser porous zone at the windward surface of the apex-facing triangular cylinder is the cause for convergent flow pattern in the porous zone. At higher buoyancy level, side-facing triangular cylinder produces lesser drag forces than apex-facing case. However, rich thermal performances are observed for apex-facing triangular configuration irrespective to the momentum of the fluid and permeability level.

- In natural convection, the increment in permeability enhances the kinetic energy of the fluid in and around it for a same value of Ra. The flow deviates heavily in the porous zone at higher aspect ratio, and it offers enormous changes in the flow behaviour at annular gap. The reduction in aspect ratio aids for the development of narrow thermal plume which significantly enhances the heat dissipation. Also, the isotherm pattern suggest that the *SOE* configuration possesses relatively higher amount of denser fluid than *SOS*.
- The magnetic field has shown strong impact on the reduction of velocity fields at annular space, and it is seen to be minor in porous zone. The overall heat transfer performance of apex-facing up configuration is observed to be higher than that of apex facing-down configuration for all values of Ra, Da and Ha. Also, the effect of permeability on heat transfer enhancement is higher in apex-facing up permeable triangular cylinder than apex-facing down case, irrespective to the intensity of magnetic field. On the other hand, the heat transfer reduction due to the augmentation in magnetic field strength is observed to be less in apex-facing down configuration.

References

[1] D. Reay, Heat transfer enhancement—A review of techniques and their possible impact on energy efficiency in the U.K., Heat Recovery Systems and CHP 11 (1) (1991) 1–40.

[2] S. Y. Kim, J. W. Paek, B. H. Kang, Flow and heat transfer correlations for porous fin in a plate-fin heat exchanger, Journal of Heat Transfer 122 (3) (2000) 572.

[3] S. Kiwan, M. A. Al-Nimr, Using porous fins for heat transfer enhancement, Journal of Heat Transfer 123 (4) (2001) 790.

[4] A. A. Mohamad, Heat transfer enhancements in heat exchangers fitted with porous media Part I: constant wall temperature, International Journal of Thermal Sciences 42 (4) (2003) 385–395.

[5] S. Bhattacharyya, S. Dhinakaran, A. Khalili, Fluid motion around and through a porous cylinder, Chemical Engineering Science 61 (13) (2006) 4451–4461.

[6] S. Dhinakaran, J. Ponmozhi, Heat transfer from a permeable square cylinder to a flowing fluid, Energy Conversion and Management 52 (5) (2011) 2170–2182.

[7] D. J. Krishna, M. R. Thansekhar, S. P. Venkateshan, T. Basak, S. K. Das, Natural convection in a partially heat generating rod bundle inside an enclosure, Journal of Heat Transfer 132 (10) (2010) 102501.

[8] A. A. Mohamad, Lattice Boltzmann method: Fundamentals and engineering applications with computer codes, Springer Science & Business Media, London Dordrecht Heidelberg New York, 2011.

[9] N. Sharma, A. K. Dhiman, S. Kumar, Mixed convection flow and heat transfer across a square cylinder under the influence of aiding buoyancy at low Reynolds numbers, International Journal of Heat and Mass Transfer 55 (9-10) (2012) 2601–2614.

[10] S. Srikanth, A. Dhiman, S. Bijjam, Confined flow and heat transfer across a triangular cylinder in a channel, International Journal of Thermal Sciences 49 (11) (2010) 2191–2200.

LIST OF PUBLICATIONS

[1] **T.R. Vijaybabu**, K. Anirudh, and S. Dhinakaran. Mixed convective heat transfer from a permeable square cylinder: A lattice Boltzmann analysis. International Journal of Heat and Mass Transfer 115 (2017): 854-870. (I.F. - 3.458)
[2] **T.R. Vijaybabu.**, K. Anirudh, and S. Dhinakaran. Lattice Boltzmann simulations of flow and heat transfer from a permeable triangular cylinder under the influence of aiding buoyancy. International Journal of Heat and Mass Transfer 117 (2018): 799-817. (I.F. - 3.458)
[3] **T.R. Vijaybabu**, K. Anirudh, and S. Dhinakaran. LBM simulation of unsteady flow and heat transfer from a diamond-shaped porous cylinder. International Journal of heat and mass transfer 118 (2018): 267-283. (I.F. - 3.458)
[4] **T.R. Vijaybabu** and S. Dhinakaran. Entropy generation for natural convection from a square porous body placed in an enclosure at different aspect ratios and alignments: an LBM study. International Journal of heat and mass transfer (communicated).
[5] **T.R. Vijaybabu** and S. Dhinakaran. LBM simulation of MHD natural convection heat transfer of Al_2O_3-water nanofluid in a horizontal square enclosure with an inner permeable triangular cylinder. International Journal of heat and mass transfer (communicated).